Inorganic Chemistry

ARTICLE

pubs.acs.org/IC

Morphology-Controllable Synthesis of Cobalt Oxalates and Their Conversion to Mesoporous Co_3O_4 Nanostructures for Application in Supercapacitors

Dewei Wang,[†,‡] Qihua Wang,[*,†] and Tingmei Wang[†]

[†]State Key Laboratory of Solid Lubrication, Lanzhou Institute of Chemical Physics, Chinese Academy of Sciences, Lanzhou, 730000, People's Republic of China, and

[‡]Graduate School of Chinese Academy of Sciences, Beijing, 10039, People's Republic of China

Supporting Information

ABSTRACT: In this work, one-dimensional and layered parallel folding of cobalt oxalate nanostructures have been selectively prepared by a one-step, template-free, water-controlled precipitation approach by simply altering the solvents used at ambient temperature and pressure. Encouragingly, the feeding order of solutions played an extraordinary role in the synthesis of nanorods and nanowires. After calcination in air, the as-prepared cobalt oxalate nanostructures were converted to mesoporous Co_3O_4 nanostructures while their original frame structures were well maintained. The phase composition, morphology, and structure of the as-obtained products were studied in detail. Electrochemical properties of the Co_3O_4 electrodes were carried out using cyclic voltammetry (CV) and galvanostatic charge−discharge measurements by a three-electrode system. The electrochemical experiments revealed that the layered parallel folding structure of mesoporous Co_3O_4 exhibited higher capacitance compared to that of the nanorods and nanowires. A maximum specific capacitance of 202.5 F g^{-1} has been obtained in 2 M KOH aqueous electrolyte at a current density of 1 A g^{-1} with a voltage window from 0 to 0.40 V. Furthermore, the specific capacitance decay after 1000 continuous charge−discharge cycles was negligible, revealing the excellent stability of the electrode. These characteristics indicate that the mesoporous Co_3O_4 nanostructures are promising electrode materials for supercapacitors.

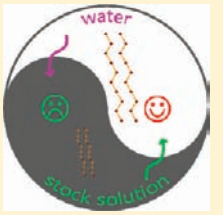

1. INTRODUCTION

With the rapid advancement of nanotechnology and related applications, the controllable and selective synthesis of nanomaterials are gradually becoming more important due to their unique physical and chemical properties, which are substantially different from those of bulk materials.[1−5] Meanwhile, synthesis and fabrication of functional nanomaterials with controlled size and shape have attracted the widespread interest of the world because the performance and properties of nanomaterials depend intimately on these two parameters.[6−9] To this end, there were increasing attempts to develop cost-effective methods to the synthesis of various nanomaterials with controllable shapes and composition in order to modify or promote their intrinsic properties.[10−12] Particularly, Co_3O_4 nanomaterials have attracted special attention because of their fascinating properties and potential applications in wide-ranging sectors including gas sensors, active materials for electrochemical energy storage and conversion, heterogeneous catalysts, electrochromic devices, solar energy absorbers, and magnetic materials.[13−19] Much research effort has therefore been devoted to designing effective methods to synthesize Co_3O_4 nanomaterials with controllable microstructures. Diverse synthetic methods, such as hydrothermal/solvothermal methods, precursor conversion processes, chemical vapor deposition synthesis, and soft-chemical growth routes have been employed to prepare various Co_3O_4 micro/nanostructures with different morphologies including nanosheets, nanocubes, nanotubes, nanoboxes, and nanobelts.[20−30] These Co_3O_4 nanostructures have a number of outstanding properties that are superior to their bulk counterparts. For example, Co_3O_4 nanorods display surprisingly high catalytic activity for CO oxidation at low temperature.[17] 1D Co_3O_4 nanostructures also exhibit improved lithium storage properties as well as promising capacitive properties.[31−35] Co_3O_4 nanosheets have large specific capacitance up to 92 F g^{-1} when used as supercapacitors.[36] However, Co_3O_4 is cubic with normal spinel structure, which lacks structural anisotropy for their 1D or 2D growth. Therefore, a soft/hard template-assisted or magnetic-field-induced route has been used for fabrication of Co_3O_4 nanostructures with confined dimension. For instance, Co_3O_4 nanotubes have been synthesized using anodic aluminum oxide membranes.[37,38] Co_3O_4 nanowires have been obtained via a magnetic-field-induced hydrothermal route.[39] Alternatively, a morphology-conserved transformation from precursor route has proven to be a promising approach for the synthesis of Co_3O_4 nanostructures. Recent studies on solid-state pyrolysis of well-designed precursors into unique porous Co_3O_4 nanostructures demonstrated the existence of a close relationship between precursor and product, which further stimulated the concept of precursor-controlled thermolysis toward defined Co_3O_4 nanostructures. Co alkoxides,[40,41] carbonates,[42,43] hydroxides,[44−46] hydroxide carbonate,[47] and oxalates[48] are often used as solid precursors to synthesize nanostructured

Received: December 6, 2010
Published: June 14, 2011

Co_3O_4 after chemical/thermal conversion. For example, Yao and co-workers described an interesting approach to prepare multi-shelled Co_3O_4 hollow spheres via calcination of Co alkoxide precursor, which has been prepared by a polymer-assisted solvothermal method.[40] Qian and co-workers synthesized one-dimensional arrays of Co_3O_4 nanoparticles by means of the thermal treatment of cobalt oxalate nanorods, which were synthesized through a convenient solvothermal route.[48] Very recently, Lou and co-workers reported a facile solvothermal approach for the shape-controlled synthesis of porous Co_3O_4 by thermal conversion of the corresponding cobalt carbonate/hydroxide intermediates.[49]

As one of the solid precursors, cobalt oxalates are potential candidates that can be used as precursor salts to produce nanoporous Co_3O_4 due to their easy synthesis, low cost, good structure stability, and relatively low decomposition temperature in air.[50] For instance, a microwave-assisted solution route has been developed by Zhu and co-workers to synthesize cobalt oxalate nanorods in the presence of ionic liquid; after calcination in air, porous Co_3O_4 nanorods were obtained.[51] Co_3O_4 nanoparticles, nanorods, and nanowires were obtained via thermal decomposition of cobalt oxalate nanorods/nanowires precursor, which were all synthesized through a microemulsion-mediated method.[52−55] Obviously, preparation of those nanostructures involves relatively complicated synthetic processes, such as a long time of solvothermal treatment, surfactants, and ion liquid. Besides, they cannot be produced on a large scale and cheaply, which largely hinders their practical use. Overall, it is more desirable to develop an alternative method to replace the microemulsion or solvothermal methods for synthesizing cobalt oxalate with controllable shapes.

As we know, the ion-exchange reaction between the cobalt ion and the oxalate ion is very rapidly in aqueous solution, which does not favor controlling the shape of the cobalt oxalates. Nevertheless, this could be circumvented by conducting the reaction in organic solvent. In organic solvent medium, the cobalt ion and the oxalic acid do not react immediately because they have a large different ionization ability. Cobalt salt, such as $CoCl_2$, can be soluble in polar solvents in the form of solvate. Oxalic acid, however, is a weak electrolyte that cannot be electrolytically dissociated into ions; instead, it governs in the form of oxalic acid in organic solvent.[56] Therefore, the ion-exchange reaction has been restrained to some extent. As water is introduced, water will gradually coordinate with cobalt ions because water has a large ligand field strength.[57] At same time, oxalic acid will dissociate into oxalate and hydronium ion; then hydrated cobalt ions can react with oxalate ion to form cobalt oxalate. The whole reaction can be described as

$$[Co(solvent)_n]^{2+} \underset{-H_2O}{\overset{+H_2O}{\leftrightarrow}} [Co(H_2O)_n]^{2+} + solvent \quad (1)$$

$$H_2C_2O_4 + H_2O \leftrightarrow H_3O^+ + HC_2O_4^- \quad (2)$$

$$HC_2O_4^- + H_2O \leftrightarrow H_3O^+ + C_2O_4^{2-} \quad (3)$$

$$[Co(H_2O)_n]^{2+} + C_2O_4^{2-} \rightarrow CoC_2O_4 \cdot 2H_2O \downarrow \quad (4)$$

From the above equations, we can see clearly that water has a profound influence on the whole reaction. Equations 1, 2, and 3 are invertible depending on the water content, while eq 4 is an irreversible reaction. With water introduced, the reaction equilibrium shifts toward the right. Thus, they can react with each other to give cobalt oxalate, which is largely insoluble in organic solvent or water at room temperature. Meanwhile, water will compete against solvent molecules to coordinate with cobalt ions, which can provide a kinetic factor for shape control. To date, however, no report has mentioned this concept to control the shape of the cobalt oxalate nanostructures, which should be simpler, quicker, and more economical for industrial applications. Most importantly, to the best of our knowledge, the extraordinary role of the feeding order of solutions and the choice of solvents in the synthesis of cobalt oxalate nanostructures were also revealed for the first time. Herein, we report a simple and robust approach based on a water-controlled precipitation strategy to synthesize cobalt oxalate with different shapes by simply altering the solvents used and the feeding manner of the solvents. After calcination in air, the as-prepared cobalt oxalates subsequently convert to mesoporous Co_3O_4 nanostructures while their original morphologies have been well maintained. To shed light on their potential applications, the as-prepared Co_3O_4 nanostructures have been applied in electrode materials for supercapacitors, which exhibit large specific capacitances and good cyclability.

2. EXPERIMENTAL SECTION

Growth of cobalt oxalates was realized through the water-controlled precipitation process. Two different methods were used for the one-step synthesis of 1D cobalt oxalate nanostructure, i.e., the water/stock solution route and the stock solution/water route. In this study, we used water as the precipitation reagent, and the stock solutions were prepared by dissolving an equal mole ratio of $H_2C_2O_4$ and $CoCl_2$ as *N,N*-dimethylacetamide (DMA) or dimethyl sulphoxide (DMSO) to form a transparent blue solution.

All chemical reagents (analytical grade) were used as received without further purification. Deionized water was used throughout.

2.1. Synthesis of Cobalt Oxalate Nanorods and Nanowires. In a typical water/stock solution route, 1 mmol of oxalic acid ($H_2C_2O_4$) was dissolved in 15 mL of *N,N*-dimethylacetamide (DMA) to form a homogeneous solution under continuous magnetic stirring. Then, 1 mmol of cobalt chloride hexahydrate ($CoCl_2 \cdot 6H_2O$) was introduced into the solution when the $H_2C_2O_4$ were dissolved completely, followed by dropwise adding 10 mL of deionized water. After stirring for 5 min, the as-prepared pink-colored precipitate was separated by centrifugation and washed with ethanol for several times and dried in a vacuum at 60 °C for 12 h. For the stock solution/water route, the synthetic procedure was identical with that for the water/stock solution route except for the feeding order of the two solutions, i.e., the stock solution was added dropwise into water under continuous magnetic stirring.

2.2. Synthesis of Layered Parallel Folding Nanostructures (LPF Nanostructures). A 2 mmol amount of $H_2C_2O_4$ was dissolved in 15 mL of dimethyl sulfoxide (DMSO) to form a homogeneous solution under continuous magnetic stirring. Then, 2 mmol of cobalt chloride hexahydrate ($CoCl_2 \cdot 6H_2O$) was introduced into the solution when $H_2C_2O_4$ was dissolved completely, followed by dropwise adding 5 mL of deionized water. The following synthetic procedure was similar to that described above.

2.3. Synthesis of Mesoporous Co_3O_4 Nanostructures. The as-prepared cobalt oxalate nanostructures were placed in a quartz boat, and then the quartz boat was placed in a muffle furnace and calcined at 400 °C for 3 h in air to obtain the Co_3O_4 nanostructures. The heating rate during calcinations should be controlled to be as low as 2 °C min^{-1}. For simplicity, the as-obtained samples were labeled as samples C1 (nanorods), C2 (nanowires), and C3 (LPF nanostructures).

2.4. Characterization. The phase structure of the products was measured by powder X-ray diffraction (XRD) experiments on a RigaKu

dx.doi.org/10.1021/ic200309t |*Inorg. Chem.* 2011, 50, 6482–6492

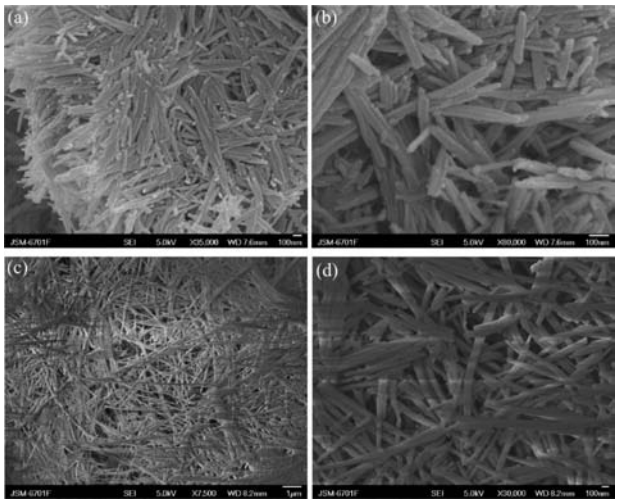

Figure 1. FESEM images of cobalt oxalate nanorods and nanowires prepared via the (a, b) water/stock solution route and (c, d) stock solution/water route (DMA as the solvent).

D/max-RB diffractometer with Ni-filtered graphite-monochromatized Cu Kα radiation (λ = 1.54056 Å). The morphology and particle sizes were observed by field emission scanning electron microcopy (FESEM, JEOL JSM-6701F). High-resolution transmission electron microscopy (HRTEM) studies were carried out on FEITECNAIF TEM (FEI, Tecnai 30) operating at an acceleration voltage of 300 kV. Samples were prepared by first dispersing the final powder in ethanol through ultrasonic treatment, and the dispersion was dropped on a carbon-coated copper grid, drying the samples in air for observation. TEM images, high-angle annular dark field scanning transmission election microscopy (HAADF-STEM) image, selected-area electron diffraction (SAED), and energy-dispersive spectroscopy (EDS) were also taken by FEI transmission electron microscopy. The Fourier transform-infrared (FT-IR) spectrum was measured on a Nicolet Nexus 870 FT-IR spectrophotometer from 4000 to 400 cm^{-1} using a KBr wafer at room temperature. A X-ray photoelectron spectrometer (XPS, VG ESCALAB 210) was carried out with Al Kα as the excitation source; the binding energies obtained in XPS analysis were calibrated against the C 1s peak at 285.0 eV. The specific surface area was estimated by the Brunauer–Emmet–Teller (BET) method based on nitrogen absorption–desorption (Micromeritics ASAP 2020).The desorption isotherm was used to determine the pore size distribution via the Barret–Joyner–Halender (BJH) method. Thermogravimetric-differential scanning calorimetric (TG-DSC) analysis of the cobalt oxalate precursor was performed on a Netzsch STA-409 PG/PC thermogravimetric analyzer (Germany). The TG and DSC curves were recorded in a dynamic atmosphere at a heating rate of 10 °C min^{-1} in the temperature range of 30–500 °C.

2.5. Electrochemical Characterization. The working electrodes were prepared by mixing the electroactive material (Co_3O_4, 75 wt %), acetylene black (15 wt %), and poly(tetrafluoroethylene) (10 wt %) binders in *N*-methyl-2-pyrrolidinone (NMP) solvent to form a homogeneous slurry, which was then pressed onto a nickel grid (about 1 × 1 cm^2) and dried at 100 °C overnight. The electrochemical measurements were done in a three-electrode cell with Pt foil (1 × 1 cm^2) as the counter electrode and a saturated calomel electrode (SCE) as the reference electrode. The used electrolyte was 2 M aqueous KOH solution. CV tests were done between −0.2 and 0.5 V (vs SCE) at different scan rates of 5, 10, and 30 mV s^{-1}. The long-term galvanostatic charge–discharge was evaluated with a LAND CT2001A multichannel galvanostat in the potential range of 0–0.4 V (vs SCE) at a current density of 1 A g^{-1}. Electrochemical impedance spectroscopy (EIS) was carried out in the frequency range from 100 kHz to 0.1 Hz at open-circuit potential with an AC perturbation of 5 mV. Cyclic voltammetry (CV) and chronopotentiometry (CP) tests were employed on an electrochemical workstation (CHI 660B, Chenhua, Shanghai). Before electrochemical tests, the working electrodes were aged for 12 h to ensure good soakage of the Co_3O_4 particles in the electrolyte.

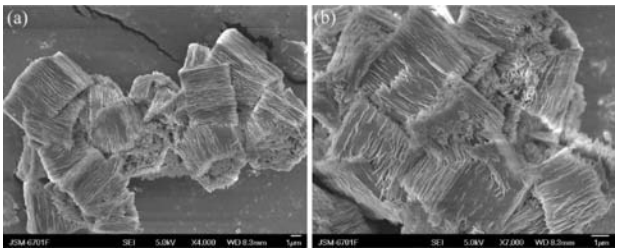

Figure 2. FESEM images of cobalt oxalate nanostructures produced via the water/stock solution route (DMSO as the solvent).

3. RESULTS AND DISCUSSION

3.1. Synthesis of Cobalt Oxalate Nanostructures. The synthesis of cobalt oxalate nanostructures was realized by changing the feeding order of the two solutions as well as the solvent selected at ambient temperature and pressure. According to the feeding order of the two solutions, two different synthesis routes were adopted: the water/stock solution route where water was added into stock solution, and the stock solution/water route where stock solution was added into water. The morphology and particle sizes were first determined by FESEM. Figure 1a and 1b shows typical FESEM images of the as-prepared cobalt oxalate nanorods produced via the water/stock solution route (DMA as the solvent). The as-obtained products were all nanorods with a diameter about 50 nm and length of about several hundred nanometers. Amazingly, when the feeding order of the two solutions was altered, nanowires were obtained. As shown in Figure 1c and 1d, the diameter of the nanowires was about 100 nm and the length was up to tens of micrometers. Strikingly, when the solvent of the stock solution was changed to DMSO, a significant change in the morphology of the produced cobalt oxalate nanostructures occurred. Figure 2a and 2b shows typical FESEM images of the as-prepared cobalt oxalate nanostructures produced via the water/stock solution route (DMSO as the solvent). As shown in Figure 2, the products were composed of many layered parallel folding structures approximately 2 μm in length, which were built from many curved sheets with a thickness of about 50 nm. However, when the feeding order of the two solutions was altered, irregular nanobelt-bundles were obtained (Figure S1, Supporting Information). A nanobelt-bundle with a diameter of about 500 nm is composed of several nanobelts with a thickness of about 50 nm with different length. The high-magnification FESEM image of the sample revealed that these rods were actually bundles of nanobelts, which were stacked in a parallel fashion.

The crystal structure of the as-synthesized cobalt oxalate powder was characterized by X-ray diffraction (XRD), with the results shown in Figure 3. As indicated by patterns a and b, all diffraction peaks show characteristics of the cobalt oxalate hydrate phase, which can be indexed to the orthorhombic phase of $CoC_2O_4 \cdot xH_2O$ (JCPDS No. 25-0250). However, the crystalline is lower than that prepared from the solvothermal/hydrothermal method since the diffraction peak for the (113) plane at

dx.doi.org/10.1021/ic200309t |*Inorg. Chem.* 2011, 50, 6482–6492

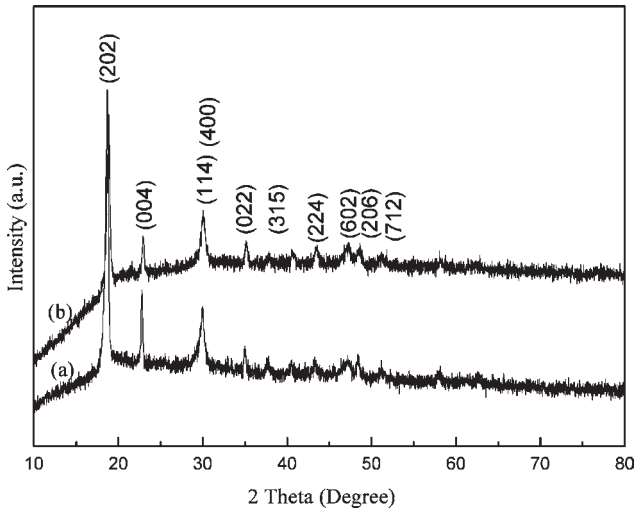

Figure 3. XRD patterns of the as-prepared cobalt oxalate nanorods (a) and nanowires (b).

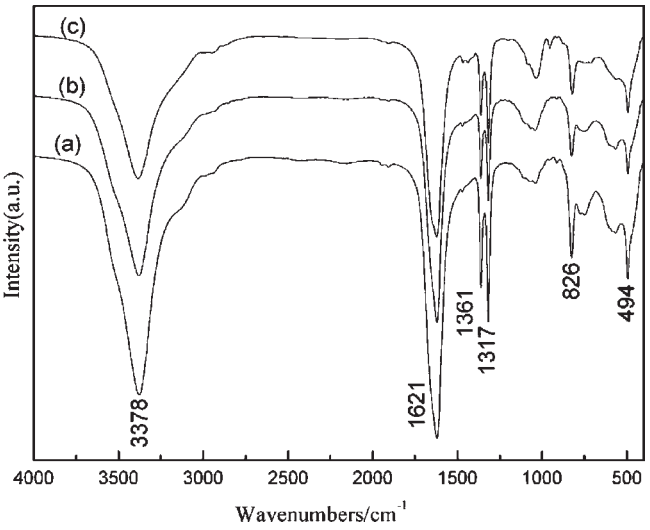

Figure 4. FT-IR spectrum of the as-prepared cobalt oxalate nanostructures (a) LPF nanostructures, (b) nanorods, and (c) nanowires.

around 25° and the other peaks could not be clearly identified, probably due to the relatively lower reaction temperature and the relatively fast reaction speed. When the reaction was conducted in DMSO, the crystalline structure could not be identified to any known phase on the basis of the JCPDS reference database (Figure S2, Supporting Information). According to the FT-IR spectrum, however, the as-prepared product gives a spectrum characteristic for the presence of hydrated metal oxalates.[53] As can be seen in Figure 4a, a strong peak at 1621 cm^{-1} is attributed to the C═O stretching vibration and the peaks at 1361 and 1317 cm^{-1} are ascribed to C−O asymmetric and symmetric vibrations, respectively, indicating the presence of bridging oxalates with all four oxygen atoms coordinated to the metal atoms.[53] The asymmetric O−C−O band appears at 826 cm^{-1}, while the broad band at 494 cm^{-1} is assigned to Co−O and symmetric C−C−O. The broad band at 3378 cm^{-1} is assigned to the water of hydration. From Figure 4, the FT-IR spectrum of the three samples are barely changed, which confirms the chemical bonding characteristic of the obtained precursor compounds are similar. The layered structure obtained from DMSO solvent may be a derivative of cobalt oxalates. From the results of the XRD and IR spectrum, it can be seen that $CoC_2O_4 \cdot xH_2O$ could be successfully obtained at such a simple route. Nevertheless, structural analysis should be under scrutiny in the future.

In present work, anisotropic cobalt oxalate nanostructures were synthesized at ambient temperature and pressure without any surfactants. Cobalt oxalate with a diversity of well-defined morphologies was synthesized through simply altering the solvents used and the feeding manner of the solvents. Generally, anisotropic growth of the crystal structure is a result of a large difference in surface energy between the crystallographic planes.[6] There are several aspects, such as highly anisotropic crystal structures, orientation attachment, surfactants/capping reagents, templates, catalysts, and self-assembly, that are key factors for anisotropic 1D growth.[4,6,12] From a structure point of view, two $C_2O_4^{2-}$ could chelate with Co^{2+} to form a square planar configuration with Co^{2+} in the center. There were two coordinated H_2O molecules at each side of the molecular plane, and two molecular planes were connected by the H_2O molecule. As a result of the hydrogen bonding as well as the $\pi-\pi$ interaction within the adjacent molecules, the growth direction parallel to the molecule planes has been heavily retarded and the growth direction perpendicular to the planes had the priority to fast growth.[58] Thus, square planes would stack face-to-face, resulting in a one-dimensional columnar structure, which could lead to formation of cobalt oxalate nanorods (Figure S3, Supporting Information).[59] Besides the anisotropic structure which induced crystallization to occur along a certain axis, the solvents used in this synthesis should also have key effects on formation of cobalt oxalate nanorods. Because of the variation in solubility, nucleation, and growth of the resultants, reaction kinetics, solution properties, and stability of the particles in different solvent systems lead to formation of nanostructures with different shapes.[60,61] Therefore, the changes of the solvents could change nucleation and growth significantly, which would change the structure of the products accordingly. Moreover, because the solvation and coordination effects of different solvents are totally different, the manner and generation speed of cobalt oxalate seeds are different, which also play an indispensable role. Particularly, when the stock solutions were added into water, anisotropic 1D growth became more notable. In the DMA solution, when the stock solution added into water, the diameters and length of the nanorods were both increased (see Figure 1). Similarly, when the DMSO stock solution was added into water, the nanobelt-bundles were obtained instead of LPF nanostructures. Why did the different feeding order of the solution have a tremendous influence on the shape of the product? In the current experiment, water has been considered to have multifold roles in the whole reaction process. First, it can act as the precipitation reagent to precipitate the cobalt oxalate because the cobalt oxalate hardly dissolved in water at room temperature. Second, water will compete with solvent molecules to coordinate with cobalt ions, which could act as a cobalt ion reservoir to balance the concentration of $[Cosolvent]^{2+}$ species in the solution, which will regulate the supersaturation concentration of Co^{2+} species in an effective way.[62] Third, water also participated in the reaction because the product cobalt oxalate has two moles of water per empirical formula (see the following section). When the stock solutions were added into water, precipitation reagent was abundant; thus, the cobalt oxalates could more easily precipitate than that the water

dx.doi.org/10.1021/ic200309t |*Inorg. Chem.* 2011, 50, 6482–6492

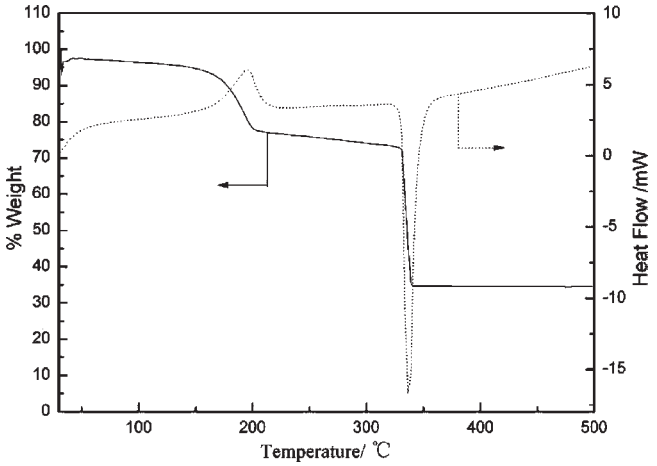

Figure 5. Thermogravimetric analysis (TGA, solid line) and differential scanning calorimetric (DSC, dotted line) plots of the cobalt oxalate nanorods in air from 30 to 500 °C at a rate of 10 °C min^{-1}.

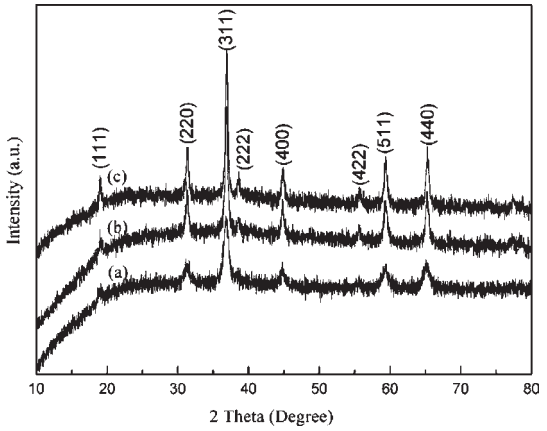

Figure 6. XRD patterns of the as-obtained Co_3O_4 nanostructures from different cobalt oxalate nanostructures (a) LPF nanostructures, (b) nanorods, and (c) nanowires.

added into stock solutions. Therefore, water could give a high chemical potential for anisotropic growth, as the water was plentiful the anisotropic growth strengthened accordingly.[63] Furthermore, we found that the pink-colored product immediately been formed as water was added in, implying that the rate of formation is quite fast. Therefore, it would be difficult to carry out a kinetic study of the shape evolution. On the basis of the above discussion, we conclude that the morphologies of resultant structures were determined by the solvents and, more importantly, the feeding order of the solvents. The proposed growth mechanism would shed new light on the study of the formation processes of other metal oxalates.

Thermogravimetric analysis (TGA) was carried out to investigate the thermal behavior of the $CoC_2O_4 \cdot xH_2O$ precursor in air. The TGA curve of the cobalt oxalate nanorods is shown in Figure 5. It can be seen that there are two distinct weight loss steps. The first weight loss occurs at 160−190 °C, which corresponds to evaporation of structural water, that is, $CoC_2O_4 \cdot xH_2O$ is converted to anhydrous cobalt oxalate in this stage. A broad endothermal peak appears in the corresponding DSC curve. About 19.9% weight loss is obtained, and this is consistent

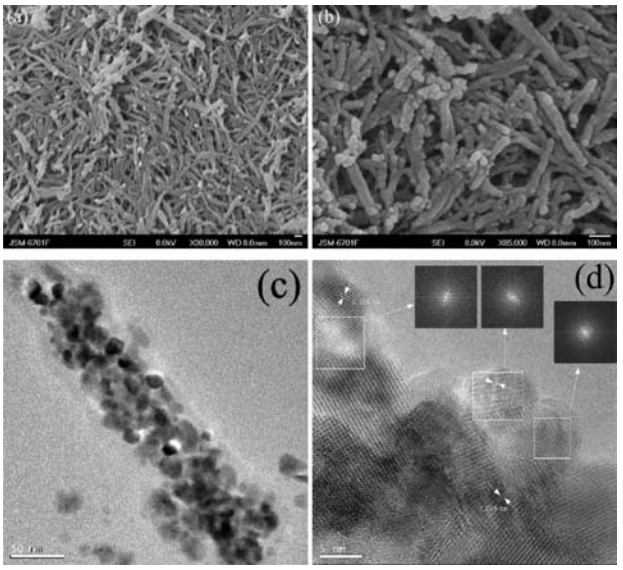

Figure 7. Morphological and structural characterization of sample C1: (a, b) FESEM images, (c) TEM image, and (d) HRTEM image. The inset of d corresponds to its fast Fourier transform (FFT) pattern taken from the selected area marked by a square.

with a calculated weight loss of 19.7%, which is attributed to complete dehydration of two water molecules. Therefore, the molecular formula is confirmed to be $CoC_2O_4 \cdot 2H_2O$. The second weight loss occurs at around 200−350 °C with an exothermal peak in the DSC curve, leading to conversion of anhydrous cobalt oxalate to Co_3O_4. The weight loss of this step is about 40%, which is close to the theoretical value. However, for LPF nanostructures, the decomposition temperature is slightly higher than the other two samples and the weight loss that is slightly lower than the theoretical value (Figures S4 and S5, Supporting Information). This is probably due to their relatively large size, which makes them more robust to decomposition.[49] On the basis of the TGA results, the temperature for calcination of the cobalt oxalate precursors to Co_3O_4 was set at 400 °C for 3 h to ensure complete decomposition of the cobalt oxalate precursors. The total decomposition process can be expressed as the following reactions

$$CoC_2O_4 \cdot 2H_2O \rightarrow CoC_2O_4 + 2H_2O \uparrow$$

$$3CoC_2O_4 + 2O_2 \rightarrow Co_3O_4 + 6CO_2 \uparrow$$

3.2. Synthesis of Co_3O_4 Nanostructures. Thermal decomposition of the precursor is a simple and common route to synthesize metal oxides. Current existing nanostructures have been considered as useful precursors to generate other nanostructures that might be difficult to synthesize directly, which means that the size and shape of the starting material are preserved during conversion.[55] On the basis of this point, when the precursors were annealed in air at 400 °C for 3 h, the as-obtained cobalt oxalates were completely converted to phase-pure spinel Co_3O_4. Figure 6 shows the representative XRD patterns of the products after heat treatment. It can be seen that all reflection peaks can be readily indexed as a pure cubic phase of Co_3O_4 (space group $Fd3m$) with a lattice constant of 8.080 Å, which is consistent with the value given in the standard card

dx.doi.org/10.1021/ic200309t |*Inorg. Chem.* 2011, 50, 6482–6492

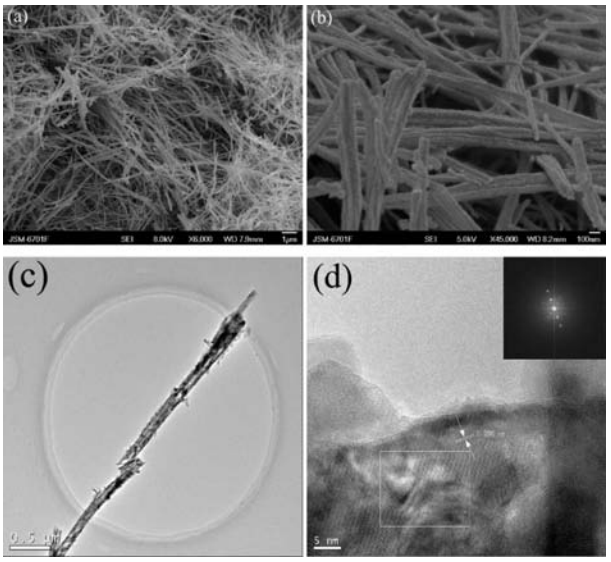

Figure 8. Morphological and structural characterization of sample C2: (a, b) FESEM images, (c) TEM image, and (d) HRTEM image. The inset of d corresponds to its FFT pattern taken from the selected area marked by a square. The fringe spacing of 0.286 nm corresponds to the (220) of cubic Co_3O_4.

(JCPDS No. 42-1467). No other impurities were detected in the XRD pattern, confirming the high purity of the products. Moreover, the XRD diffraction peaks are relatively broad, indicating that the crystals constituting the products are small in size.

Figure 7 shows the morphological and structural characterizations of sample C1 prepared by calcination of cobalt oxalate nanorods at 400 °C for 3 h. From the FESEM images, lots of rod-like Co_3O_4 nanostructures with a 50 nm in diameter and hundreds of nanometers in length are obtained by calcination. Moreover, Figure 7c shows the magnified TEM image of an individual Co_3O_4 nanorod. As can be seen, each Co_3O_4 nanorod is composed of numerous nanoparticles with a size of several nanometers, indicating that the Co_3O_4 nanorod is polycrystalline in nature. The corresponding selected area electron diffraction (SAED) pattern (Supporting Information, Figure S6) shows distinct rings, further confirming the polycrystalline nature of the as-prepared porous rod-like Co_3O_4 nanostructures. Figure 7d shows the HRTEM image; the fringe spacing of 0.47 and 0.29 nm corresponds to the (111) and (220) planes of cubic Co_3O_4. For sample C2, the FESEM and TEM images, as shown in Figure 8, indicated that the morphology of the precursor was successfully conserved as well. The Co_3O_4 nanowires are about 100 nm in diameter and tens of micrometers in length, which is consistent with the nanowires precursor. The HRTEM image (Figure 8d, Supporting Information, Figure S7) and SAED pattern (Supporting Information, Figure S8) also reveal that the nanowires are well crystalline.

Figure 9 demonstrates that the LPF nanostructures also exhibited good thermal stability and that there was not substantial morphological alteration after the annealing process except the surface of the folding structures became rougher (Figure 9a and 9b). From the TEM (Figure 9c and 9d) and HRTEM (Figure S9, Supporting Information) images, it can be observed that the folding structures are composed of numerous nanoparticles with a size of several nanometers; abundant pore structures are

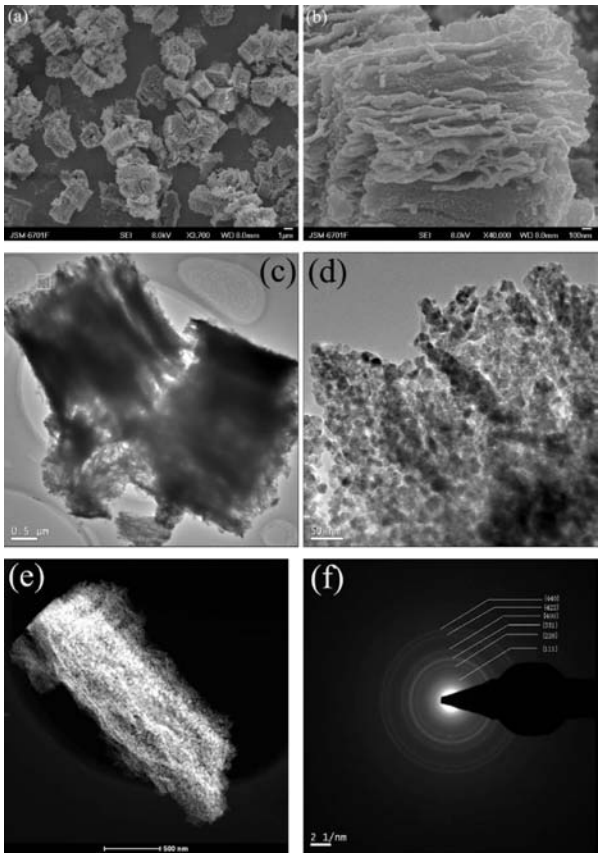

Figure 9. FESEM and TEM images of sample C3 prepared by calcination of layered parallel folding cobalt oxalate nanostructures precursor at 400 °C for 3 h: (a) lower magnification and (b) higher magnification, (c) lower magnification TEM image, (d) higher magnification TEM image taking from the rectangular area taken from the selected area marked by a square in c, (e) HAADF- STEM image, and (f) corresponding SAED pattern.

formed among the nanoparticles. From the the HAADF-STEM image (Figure 9e), a typical layered parallel folding structures is 2 μm in length with a roughed surface embeded with numerous pores in them. To the best of our knowledge, this novel folding structure has not been reported for Co_3O_4 yet. The corresponding selected area electron diffraction (SAED) pattern (Figure 9f) shows distinct rings: the rings from the innermost ring to the outside correspond to the (111), (220), (331), (400), (422), and (440) planes of the cubic phase of Co_3O_4, which are consistent with XRD results. This observation reveals the polycrystalline nature of the as-prepared layered parallel folding Co_3O_4 nanostructures.

The chemical composition of these three samples was investigated with elemental analysis by EDS. Taking sample C3 as an example, the EDS spectrum (Figure S10, Supporting Information) confirmed that the as-prepared sample consisted of Co and O elements, and the signals of the Cu element originated from the supporting HRTEM grid during the measurement. The molar ratio of Co and O is 43.96:56.03 (~3:4), within experimental error, which is consistent with the composition of Co_3O_4. The chemical bonding states in the product were further provided by X-ray photoelectron spectroscopy (XPS) measurements, as shown in Figure 10. The binding energies obtained in the XPS analysis were corrected for specimen charging, through referencing the C

dx.doi.org/10.1021/ic200309t |*Inorg. Chem.* 2011, 50, 6482–6492

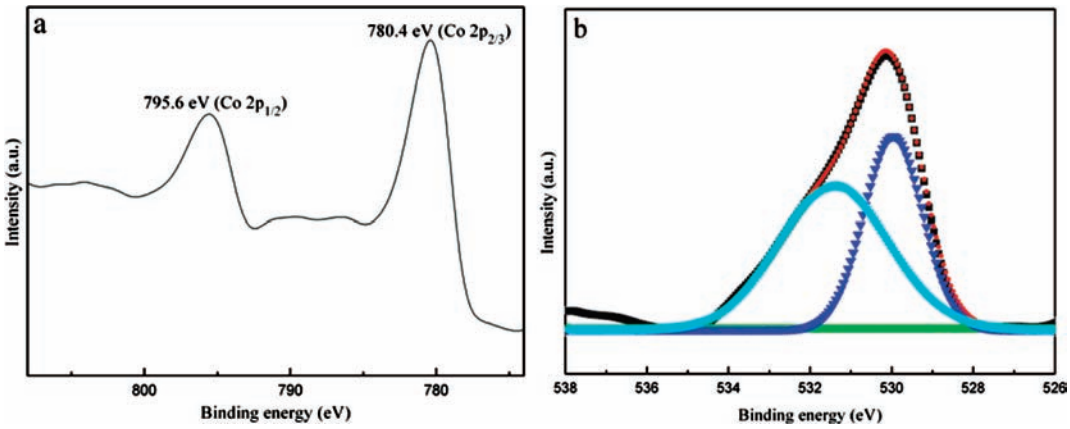

Figure 10. High-resolution XPS measurements for the (a) Co 2p and (b) O 1s core levels for sample C3.

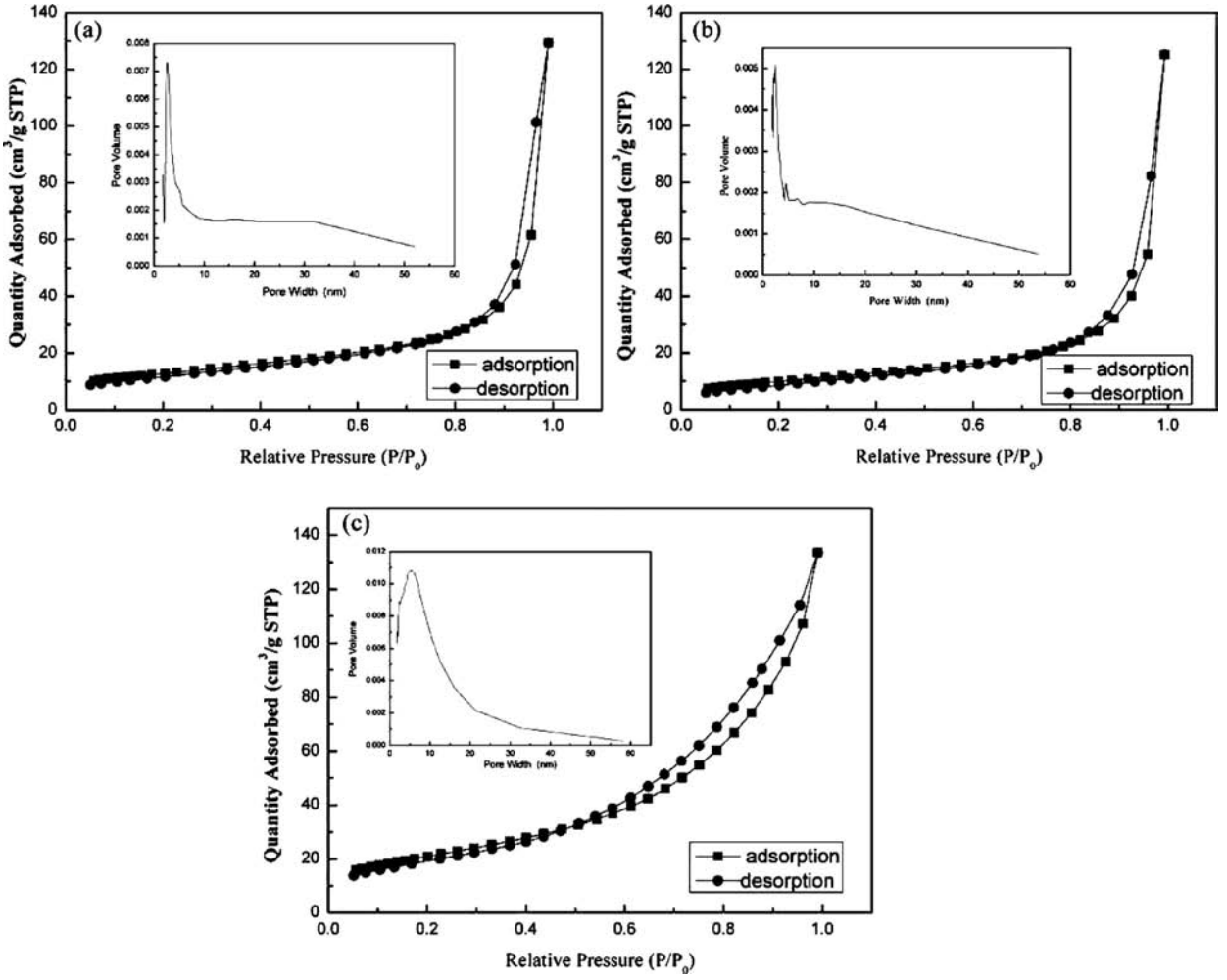

Figure 11. N_2 adsorption−desorption isotherms of samples C1 (A), C2 (B), and C3 (C). Inset in each isotherm is the corresponding pore size distributions.

1s to 285.0 eV. The Co 2p XPS spectra of the sample exhibit two peaks at 795.6 and 780.4 eV, corresponding to the Co $2p_{1/2}$ and Co $2p_{3/2}$ spin−orbit peaks of Co_3O_4 (Figure 10a).[36] Figure 10b shows the deconvoluted O 1s spectrum, where one sharp peak located at 530.1 eV and one broad peak located at 531.3 eV can be observed. The core levels were centered at 530.1 and 531.3 eV, which were assigned to oxygen species in the spinel Co_3O_4 phase and the presence of −OH species adsorbed onto the surface of the nanostructures, respectively.

To study the pore structural and the specific surface areas of the as-obtained Co_3O_4 nanostructures, Brunauer−Emmett−Teller (BET) gas-sorption measurements are carried out. Nitrogen

dx.doi.org/10.1021/ic200309t |*Inorg. Chem.* 2011, 50, 6482–6492

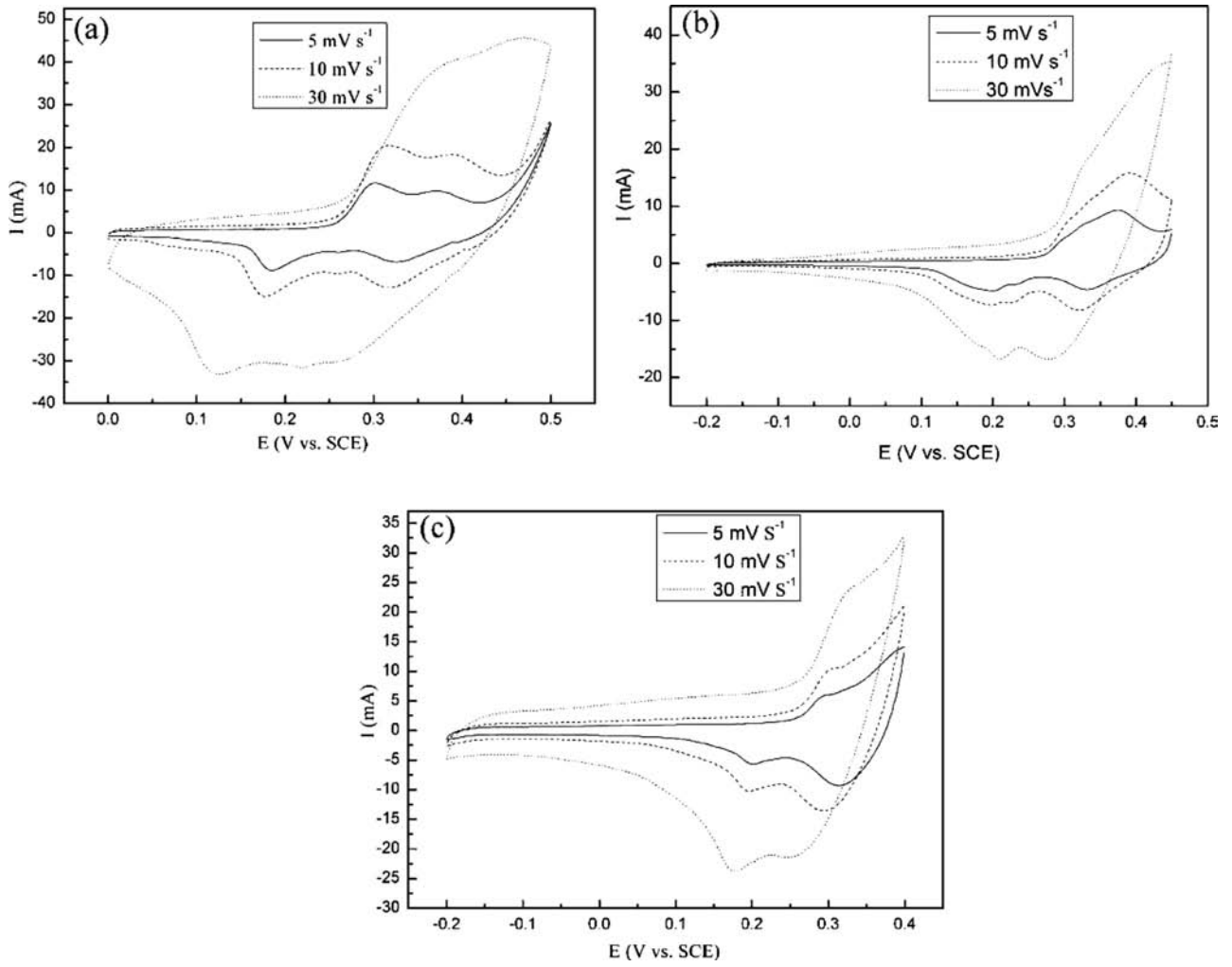

Figure 12. Cyclic voltammograms of samples C1 (a), C2 (b), and C3 (c) in 2 M KOH aqueous electrolyte at a scan rate from 5 to 30 mV s^{-1}. The voltage windows used for C1, C2, and C3 are from 0 to 0.50 V, −0.2 to 0.45 V, and −0.2 to 0.4 V, respectively.

adsorption−desorption isotherms of these samples are shown in Figure 11, and the insets show the corresponding Barrett−Joyner−Halenda (BJH) pore size distribution plots. The N_2 adsorption and desorption experiments of the samples show a typical type IV isotherm. When the relative pressure (P/P_0) is higher than 0.9, a small increase appears, indicating the secondary pores due to aggregation of particles. A distinct hysteresis loop observed at a relative pressure is different for these three samples. The BET specific surface areas of these three samples are measured to be 45.1, 35.6, and 75.9 $m^2\ g^{-1}$ for samples C1, C2, and C3, respectively, which shows that there is little difference in the specific surface area between these types of morphology. The average pore diameters were 17.28, 19.37, and 8.58 nm, for samples C1, C2, and C3, respectively, according to the BJH plots calculated from the nitrogen isotherms of the porous Co_3O_4 nanostructures.

3.3. Electrochemical Properties. Transition-metal oxides are promising candidates applicable in supercapacitors because of their easy synthesis and good capacitive characteristics. Different Co_3O_4 nanostructures were used to make supercapacitor electrodes, and their electrochemical properties were studied by means of cyclic voltammetry (CV) in a 2 M KOH electrolyte. For Co_3O_4 as an electrode material, it is believed that the surface Faradaic reaction can be expressed as follows[64]

$$Co_3O_4 + OH^- + H_2O \rightleftharpoons 3CoOOH + e^- \quad (1)$$

$$CoOOH + OH^- \rightleftharpoons CoO_2 + H_2O + e^- \quad (2)$$

Figure 12 shows the cyclic voltammograms of the three samples in 2 M KOH electrolyte at scan rates from 5 to 30 mV s^{-1}. As can be seen in Figure 12, the Co_3O_4 electrodes show the characteristic of the pseudocapacitance caused by electrochemical reactions, which is very different from that of the electric double-layer capacitance, in which the CV curve is close to the ideal rectangular shape.[35,36,49] The present results imply that the measured capacitance is mainly associated with the redox mechanism. The mechanism of electrochemical reactions of Co_3O_4 in alkaline electrolyte is still not fully understood, but the redox reaction peaks are visible in the CV curves, which can be found to be responsible for the redox process of Co_3O_4.[35] The peak current also increases with increasing scan rate from 5 to 30 mV s^{-1}; as the shape of the CV changed gradually, anodic peak potential and cathodic peak potential shift in the more anodic and more cathodic direction, which led to decreased capacitance.[65] This phenomenon can be understood by the

dx.doi.org/10.1021/ic200309t |Inorg. Chem. 2011, 50, 6482–6492

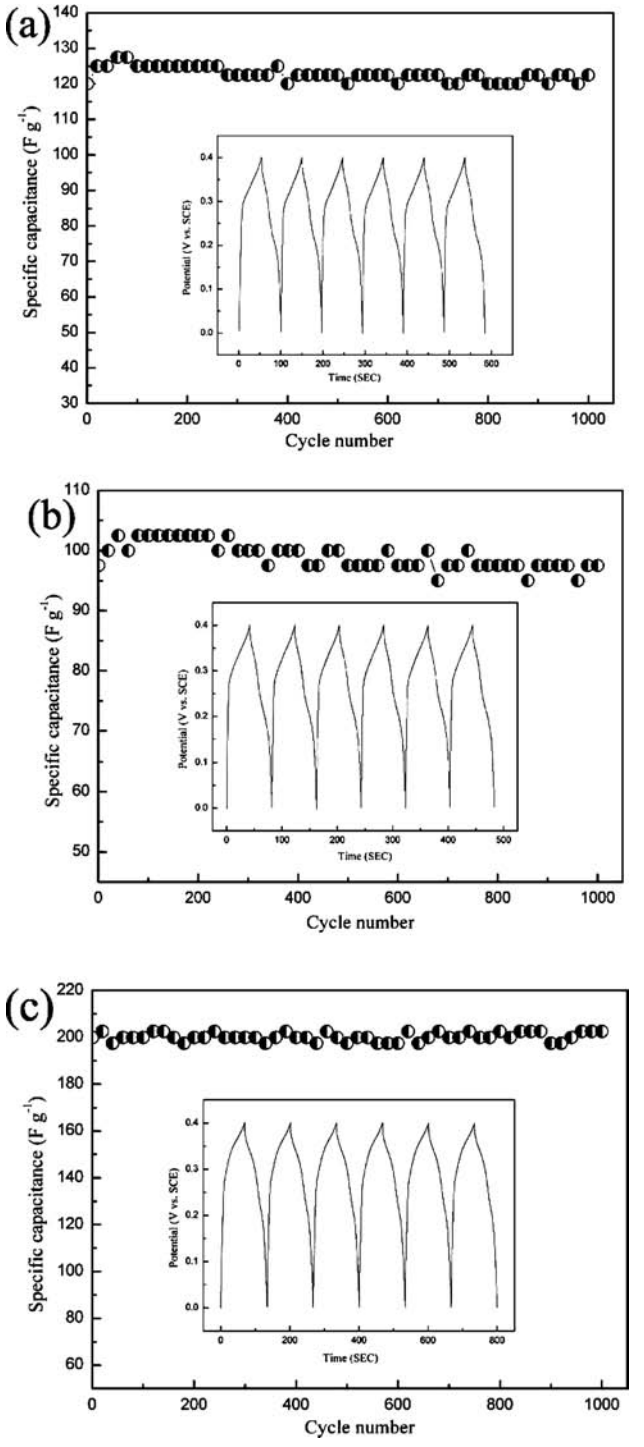

Figure 13. Specific capacitance values of samples C1 (a), C2 (b), and C3 (c) in an aqueous KOH (2 M) electrolyte as a function of cycle number. The inserts show the charge−discharge profiles of the first six charge−discharge cycles at a current density of 1 A g^{-1} with the voltage window from 0 to 0.40 V.

circuitous diffusion of OH^- ions into the pores of Co_3O_4 nanostructures as well as the electrode resistance. At high scan rates, diffusion limits the movement of OH^- ions due to time constraints and only the outer active surface is utilized for the charge storage, whereas at low scan rates all the active surface area can be utilized for charge storage and thus leads to higher specific capacitance.[66] The cyclability of the electrodes in electrolyte is one of the important aspects for their practical application. As shown in Figure 13, the specific capacitance decay after 1000 continuous charge−discharge cycles was negligible, revealing the excellent electrochemical stability of the product. The specific capacitances were calculated from the galvanostatic discharge curves using the equation: $C = It/(\Delta Vm)$, where I is the current applied, t is the total discharge time, ΔV is the potential drop during discharging, and m is the mass of the sample on one electrode. On the basis of this equation, the specific capacitance values of samples C1, C2, and C3 can thus be calculated from the discharge curves to be 127.5, 102.5, and 202.5 F g^{-1}, respectively. Inserts show the charge−discharge behavior of the samples at a current density of 1 A g^{-1} in KOH solution (2 M) within a potential range of 0 to 0.4 V (versus SCE). During the charge and discharge steps, the curves display two variation ranges. Below about 0.1 V, the time dependence of the potential is linear, indicating the pure double-layer capacitance behavior from the charge separation at the electrode/electrolyte interface.[36] Above 0.1 V, the dependence is nonlinear, indicating again the typical pseudocapacitance behavior. The symmetry of the charge and discharge characteristics and the almost constant slope of these curves further support that the electrode has high electrochemical reversibility and excellent capacitive characteristics. These well-defined 1D or 3D structures can not only improve the mechanical integrity of the electrode but also enhance the electronic conduction between particles, which will undoubtedly improve utilization of active materials. The remarkable enhancement in the specific capacitance of the sample C3 can mainly be attributed to their higher specific surface area, smaller pores, and particle size, which shorten the diffusion length of OH^- ions, leading to an improved pseudocapacitive performance.[67] Furthermore, the Faradaic charge transfer resistance for C3 is very low (Figure S11, Supporting Information), which contribute to enhancing the utilization of active materials and mitigating internal resistance of the capacitors, therefore, increasing the specific capacitance value.[68] In particular, such porous nanostructures can act as "ion-buffering reservoirs", which sustain the supply of OH^- ions and ensure that sufficient Faradic reactions can take place for energy storage.[69] These results show that these active Co_3O_4 nanomaterials have large pseudocapacitance and good reversibility, which may have potential applications in supercapacitors and lithium-ion batteries.

4. CONCLUSIONS

In summary, we designed a facile and versatile water-controlled precipitation approach for preparation of various cobalt oxalate nanostructures, including nanorods, nanowires, and layered parallel folding nanostructures. The morphologies of resultant structures are determined by the solvents and more importantly the feeding order of the solvents. After calcination in air, the as-prepared cobalt oxalate nanostructures subsequently convert to porous Co_3O_4 nanostructures while maintaining their original frame structure. Electrochemical measurements indicated that the novel porous Co_3O_4-layered parallel folding nanostructures could deliver a maximum specific capacitance of 202.5 F g^{-1} for a single electrode and good stability over 1000 cycles. The easy synthesis and short production process would be helpful in production of Co_3O_4 nanostructures on a large scale. This efficient approach demonstrated here not only could be extended for the synthesis of other metal oxides with controlled

shape and structure but also fundamentally provided a new route toward fabrication of inorganic materials into well-defined morphologies with potential applications.

■ ASSOCIATED CONTENT

Supporting Information. FESEM, TEM, HRTEM images; FFT, SAED patterns; TG-DSC studies; XRD and EDS analysis. This material is available free of charge via the Internet at http://pubs.acs.org.

■ AUTHOR INFORMATION

Corresponding Author
*Phone: +86-931-4968180. Fax: +86-931-8277088. E-mail: Wangqh@lzb.ac.cn.

■ ACKNOWLEDGMENT

The authors would like to acknowledge the financial support of the National Science Foundation for Distinguished Young Scholars of China (Grant No. 51025517), the Innovative Group Foundation of NSFC (Grant No. 50721062), and the National 973 project of China (2007CB607606).

■ REFERENCES

(1) Bruchez, M.; Moronne, J. M.; Gin, P.; Weiss, S.; Alivisatos, A. P. *Science* **1998**, *281*, 2013–2016.
(2) Tian, N.; Zhou, Z. Y.; Sun, S. G.; Ding, Y.; Wang, Z. L. *Science* **2007**, *316*, 732–735.
(3) Wang, D. S.; Xie, T.; Li, Y. D. *Nano Res.* **2009**, *2*, 30–46.
(4) Xia, Y. N.; Yang, P. D.; Sun, Y. G.; Wu, Y. Y.; Mayers, B.; Gates, B.; Yin, Y. D.; Kim, F.; Yan, H. Q. *Adv. Mater.* **2003**, *15*, 353–389.
(5) Burda, C.; Chen, X. B.; Narayanan, R.; El-Sayed, M. A. *Chem. Rev.* **2005**, *105*, 1025–1102.
(6) Jun, Y. W.; Choi, J. S.; Cheon, J. *Angew. Chem., Int. Ed.* **2006**, *45*, 3414–3439.
(7) Xia, Y. N.; Xiong, Y. J.; Lim, B.; Skrabalak, S. E. *Angew. Chem., Int. Ed.* **2009**, *48*, 60–103.
(8) Schliehe, C.; Juarez, B. H.; Pelletier, M.; Jander, S.; Greshnykh, D.; Nagel, M.; Meyer, A.; Foerster, S.; Kornowski, A.; Klinke, C.; Weller, H. *Science* **2010**, *329*, 550–553.
(9) Goesmann, H.; Feldmann, C. *Angew. Chem., Int. Ed.* **2010**, *49*, 1362–1395.
(10) Murphy, C. J.; Gole, A. M.; Hunyadi, S. E.; Orendorff, C. J. *Inorg. Chem.* **2006**, *45*, 7544–7554.
(11) Wang, X.; Zhuang, J.; Peng, Q.; Li, Y. D. *Nature* **2005**, *437*, 121–124.
(12) Wang, X.; Li, Y. D. *Inorg. Chem.* **2006**, *45*, 7522–7534.
(13) Fonseca, C. N.; DePaoli, M. A.; Gorenstein, A. *Adv. Mater.* **1991**, *3*, 553–555.
(14) Poizot, P.; Laruelle, S.; Grugeon, S.; Dupont, L.; Tarascon, J. M. *Nature* **2000**, *407*, 496–499.
(15) Park, J. S.; Shen, X. P.; Wang, G. X. *Sens. Actuators B* **2009**, *136*, 494–498.
(16) Salabas, E. L.; Rumplecker, A.; Kleitz, F.; Radu, F.; Schueth, F. *Nano Lett.* **2006**, *6*, 2977–2981.
(17) Xie, X. W.; Li, Y.; Liu, Z. Q.; Haruta, M.; Shen, W. J. *Nature* **2009**, *458*, 746–749.
(18) Barrera, E.; Viveros, T.; Montoya, A.; Ruiz, M. *J. Sol. Energy Mater. Sol. Cells* **1999**, *57*, 127–140.
(19) Liu, Y.; Zhao, W. W.; Zhang, X. G. *Electrochim. Acta* **2008**, *53*, 3296–3304.
(20) Liang, H. Y.; Raitano, J. M.; Zhang, L. H.; Chan, S. W. *Chem. Commun.* **2009**, 7569–7571.
(21) Du, N.; Zhang, H.; Chen, B.; Wu, J. B.; Ma, X. Y.; Liu, Z. H.; Zhang, Y. Q.; Yang, D.; Huang, X. H.; Tu, J. P. *Adv. Mater.* **2007**, *19*, 4505–4509.
(22) Lou, X. W.; Deng, D.; Lee, J. Y.; Feng, J.; Archer, L. A. *Adv. Mater.* **2008**, *20*, 258–262.
(23) Barreca, D.; Gasparotto, A.; Lebedev, O. I.; Maccato, C.; Pozza, A.; Tondello, E.; Turner, S.; Van Tendeloo, G. *CrystEngComm.* **2010**, *12*, 2185–2197.
(24) Yu, T.; Zhu, Y. W.; Xu, X. J.; Shen, Z. X.; Chen, P.; Lim, C. T.; Thong, J. T. L.; Sow, C. H. *Adv. Mater.* **2005**, *17*, 1595–1599.
(25) He, T.; Chen, D. R.; Jiao, X. L.; Wang, Y. L. *Adv. Mater.* **2006**, *18*, 1078–1082.
(26) Feng, J.; Zeng, H. C. *Chem. Mater.* **2003**, *15*, 2829–2835.
(27) Hu, L. H.; Peng, Q.; Li, Y. D. *J. Am. Chem. Soc.* **2008**, *130*, 16136–16137.
(28) Tian, L.; Zou, H. L.; Fu, J. X.; Yang, X. F.; Wang, Y.; Guo, H. L.; Fu, X. H.; Liang, C. L.; Wu, M. M.; Shen, P. K.; Gao, Q. M. *Adv. Funct. Mater.* **2010**, *20*, 617–623.
(29) Liu, X. H.; Qiu, G. Z.; Li, X. G. *Nanotechnology* **2005**, *16*, 3035–3040.
(30) Bandoli, G.; Barreca, D.; Gasparotto, A.; Maccato, C.; Seraglia, R.; Tondello, E.; Devi, A.; Fischer, R. A.; Winter, M. *Inorg. Chem.* **2009**, *48*, 82–89.
(31) Liu, H. J.; Bo, S. H.; Cui, W. J.; Li, F.; Wang, C. X.; Xia, Y. Y. *Electrochim. Acta* **2008**, *53*, 6497–6503.
(32) Li, Y. G.; Tan, B.; Wu, Y. Y. *Nano Lett.* **2008**, *8*, 265–270.
(33) Nam, K. T.; Kim, D. W.; Yoo, P. J.; Chiang, C. Y.; Meethong, N.; Hammond, P. T.; Chiang, Y. M.; Belcher, A. M. *Science* **2006**, *312*, 885–888.
(34) Lou, X. W.; Deng, D.; Lee, J. Y.; Archer, L. A. *J. Mater. Chem.* **2008**, *18*, 4397–4401.
(35) Cui, L.; Li, J.; Zhang, X. G. *J. Appl. Electrochem.* **2009**, *39*, 1871–1876.
(36) Xiong, S. L.; Yuan, C. Z.; Zhang, X. G.; Xi, B. J.; Qian, Y. T. *Chem.—Eur. J.* **2009**, *15*, 5320–5326.
(37) Li, W. Y.; Xu, L. N.; Chen, J. *Adv. Funct. Mater.* **2005**, *15*, 851–857.
(38) Li, T.; Yang, S. G.; Huang, L. S.; Gu, B. X.; Du, Y. W. *Nanotechnology* **2004**, *15*, 1479–1482.
(39) Wang, M. S.; Xiong, J.; Sun, Y. B.; Chen, Q. W. *CrystEngComm.* **2010**, *12*, 3262–3266.
(40) Wang, X.; Wu, X. L.; Guo, Y. G.; Zhong, Y. T.; Cao, X. Q.; Ma, Y.; Yao, J. N. *Adv. Funct. Mater.* **2010**, *20*, 1680–1686.
(41) Cao, A. M.; Hu, J. S.; Liang, H. P. *J. Phys. Chem. B* **2006**, *110*, 15858–15863.
(42) Li, C. C.; Yin, X. M.; Wang, T. H.; Zeng, H. C. *Chem. Mater.* **2009**, *21*, 4984–4992.
(43) Cong, H. P.; Yu, S. H. *Cryst. Growth Des.* **2009**, *9*, 210–217.
(44) Zhan, F. M.; Geng, B. Y.; Guo, Y. J. *Chem.—Eur. J.* **2009**, *15*, 6169–6174.
(45) Ding, Y. S.; Xu, L. P.; Chen, C. H.; Shen, X. F.; Suib, S, L. *J. Phys. Chem. C* **2008**, *112*, 8177–8183.
(46) Yang, J. H.; Hyodo, H.; Kimura, K.; Sasaki, T. *Nanotechnology* **2010**, *21*, 045605.
(47) Li, B. X.; Xie, Y.; Wu, C. Z.; Li, Z. Q.; Zhang, J. *Mater. Chem. Phys.* **2006**, *99*, 479–486.
(48) Wang, X.; Chen, X. Y.; Gao, L. S.; Zheng, H. G.; Zhang, Z. D.; Qian, Y. T. *J. Phys. Chem. B* **2004**, *108*, 16401–16404.
(49) Zhu, T.; Chen, J. S.; Lou, X. W. *J. Mater. Chem.* **2010**, *20*, 7015–7020.
(50) Yu, C. C.; Zhang, L. X.; Shi, J. L.; Zhao, J. J.; Gao, J. H.; Yan, D. S. *Adv. Funct. Mater.* **2008**, *18*, 1544–1554.
(51) Wang, W. W.; Zhu, Y. J. *Mater. Res. Bull.* **2005**, *40*, 1929–1935.
(52) Ahmed, J.; Ahmad, T.; Ramanujachary, K. V.; Lofland, S. E.; Ganguli, A. K. *J. Colloid Interface Sci.* **2008**, *321*, 434–441.
(53) Ren, L.; Wang, P. P.; Han, Y. S.; Hu, C. W.; Wei, B. Q. *Chem. Phys. Lett.* **2009**, *476*, 78–83.
(54) Xu, R.; Wang, J. W.; Li, Q. Y.; Sun, G. Y.; Wang, E. B.; Li, S. H.; Gu, J. M.; Ju, M. L. *J. Solid State Chem.* **2009**, *182*, 3177–3182.

(55) Du, N.; Xu, Y. F.; Zhang, H.; Zhai, C. X.; Yang, D. R. *Nanoscale Res. Lett.* **2010**, *5*, 1295–1300.
(56) House, J. E. *Inorganic Chemistry*; Academic Press: Burlington, 2008.
(57) Housecroft, C. E. *Inorganic Chemistry*; Pearson Education: Edinburgh Gate, 2005.
(58) Yang, L.; Wang, G. Z.; Tang, C. J.; Wang, H. Q.; Zhang, L. *Chem. Phys. Lett.* **2005**, *409*, 337–341.
(59) Pang, H.; Lu, Q. Y.; Lia, Y. C.; Gao, F. *Chem.Comm.* **2009**, 7542–7544.
(60) Guo, X. H.; Yu, S. H.; Cai, G. B. *Angew. Chem., Int. Ed.* **2006**, *45*, 3977–3981.
(61) Polleux, J.; Antonietti, M.; Niederberger, M. *J. Mater. Chem.* **2006**, *16*, 3969–3975.
(62) Wang, D. W.; Wang, Q. H.; Wang, T. M. *CrystEngComm.* **2010**, *12*, 755–761.
(63) Peng, X. G. *Adv. Mater.* **2003**, *15*, 459–463.
(64) Palmas, S.; Ferrara, F.; Vacca, A.; Mascia, M.; Polcaro, A. M. *Electrochim. Acta* **2007**, *53*, 400–406.
(65) Kong, L. B.; Lang, J. W.; Liu, M.; Luo, Y. C.; Kang, L. *J. Power Sources.* **2009**, *194*, 1194–1201.
(66) Toupin, M.; Brousse, T.; Belanger, D. *Chem. Mater.* **2002**, *14*, 3946–3952.
(67) Wang, G. X.; Liu, H.; Horvat, J.; Wang, B.; Qiao, S. Z.; Park, J.; Ahn, H. *Chem.—Eur. J.* **2010**, *16*, 11020–11027.
(68) Wu, M. S.; Hsieh, H. H *Electrochim. Acta* **2008**, *53*, 3427–3435.
(69) Wang, D. W.; Li, F.; Liu, M.; Lu, G. Q.; Cheng, H. M. *Angew. Chem., Int. Ed.* **2008**, *47*, 373–376.